Numerical Simulation of Aggregate Dispersion in Different Flow Fields Using Discrete Element Method

M. Salami Hosseini,[1] H. Nazockdast,[1] B. Dabir[2]

[1]*Polymer Engineering Department, Amirkabir University of Technology, Tehran, Iran*
[2]*Chemical Engineering Department, Amirkabir University of Technology, Tehran, Iran*

Received 12 February 2008; accepted 12 January 2009
DOI 10.1002/app.30029
Published online 3 November 2009 in Wiley InterScience (www.interscience.wiley.com).

ABSTRACT: An attempt was made to study the aggregate dispersion process in three different flow fields namely; steady shear, elongation flow, and combined shear and elongational flows using the discrete element method. The simulation was performed on two aggregate structures characterized by their fractal dimensions. The predicted results showed that the aggregate break-up process evaluated in terms of weighted average fragment size $\langle w \rangle$ follows a power–law type relation as $\langle w \rangle = kt^{-m}$ in all the three flow fields. The dispersion performance of different flow fields evaluated by dispersing rate and a final steady-state fragment size was found to be dependent upon the extent of applied stress and flow fields such that at low applied stress levels much smaller steady state values of $\langle w \rangle$ could be obtained for the elongational flow. The aggregate structure, characterized by its fractal dimension, was found to have different effects on the aggregate dispersion process depending on the flow field and applied stress level. The results predicted from this simulation could be explained in terms of ability of flow fields in rotating the aggregates and fragments in appropriate position to be broken up and the fractal dimensions of aggregates. © 2009 Wiley Periodicals, Inc. J Appl Polym Sci 115: 3303–3310, 2010

Key words: dispersion; aggregate; mixing; DEM

INTRODUCTION

The dispersive mixing process is among the most important steps in material processing particularly polymer mixing and compounding. The main objective of dispersive mixing process in polymer processing is to break down the agglomerate and/or aggregate into smaller fragments or particles by convective forces imposed by flow fields. It is generally known that the extent of dispersive mixing of aggregate plays a significant role in determining the melt processability and properties of the final product. Although numerous research works have been carried out with focus on the mechanism and parameters controlling the aggregate dispersive mixing process, the diversity of the parameters and complicated interaction between the controlling parameters have made the process too difficult to be understood.

Powell and Mason[1] studied the break-up of spherical agglomerate subjected to the shear flow and showed that the agglomerate is first deformed into the shape of an elliptic and after that, particles began to detach from the mother agglomerate. Shiga et al.[2] investigated the dispersion of carbon black agglomerates and observed that the particles detached from the mother agglomerate layer by layer and proposed the "onion model" for dispersion of the carbon black agglomerate. Feke and Manas-Zlockzower[3] proposed a model for determining of the rupture probability of spherical clusters in shear flow field. Hansen et al.[4] studied the dispersion of solid agglomerates in non-homogenous flow fields and showed that the mass fraction of ultimate size clusters can be predicted by a polynomial relation and the overall rates of erosion in either poorly or well-mixed flows can be described by a power–law relation. Horwatt et al.[5] studied the influence of structural heterogeneity on dispersion behavior of agglomerates in simple shear flow and showed that there is a power–law relation between the average fragment size and applied stress. They found that power–law exponent increases with the agglomerate fractal dimension and indicated that the fractal dimension is not sufficient to predict dispersion behavior. Rwei et al.[6,7] proposed erosion and rupture mechanisms prevailing the dispersion of carbon black agglomerates takes place in various stage of matrix diffusion into the agglomerates. Boisses and Brady[8] introduced the Stokesian dynamics to calculate hydrodynamic movement of individual particle. However, this method requires quite long time to calculate the movement of particles in an aggregate.

In recent years, numerical methods have widely been used to simulate the dispersion process of

Correspondence to: H. Nazockdast (nazdast@aut.ac.ir).

aggregate. Cundall[9,10] introduced a numerical method called as discrete element method (DEM) in which the displacement of each particle was predicted according to the balance of forces imposed on it. This simulation has been applied for many cases in powder technology e.g. the prediction of packing behavior of powders and fracture behavior of agglomerates. Higashitani et al.[11,12] has adopted this method to develop a model to predict the response of agglomerate in simple flow fields. Fanelli et al.[13,14] used this method to study the dispersion of particle cluster in nano-scale in steady and oscillated shearing fields.

In the preset study, a 2D simulation based on DEM was employed to study the dispersion of particle aggregate in different flow fields.

NUMERICAL APPROACH

DEM calculation

In the model used in the present work, the translational and rotational movements of each individual particle in aggregates subjected to flow field were calculated using DEM, in which inter-particle forces, based on the theory proposed by Derjaguin, Landau, Verwey, and Overbe (DLVO theory), as well as hydrodynamic forces were taken into account. Because in our system the *Péclet* number (Pe = $6\pi\mu\gamma a^3/kT$) is between 2600 and 8700, the Brownian force could be neglected with a good approximation. The simulation was performed on a 2D aggregate composed of N particle with radius a and density ρ in three different flow fields namely shear, elongational, and combined shear-elongational.

The particle translational and rotational motion can be expressed as:

$$m\frac{dv_i}{dt} = F_i \tag{1}$$

$$I\frac{d\omega_i}{dt} = M_i \tag{2}$$

where v_i, F_i, M_i, ω_i, I and m are velocity, total force, total torque, angular velocity, momentum of inertia, and mass of particle i respectively. The total force acting on particle i can be determined through summation over all the forces acting which can be expressed as follows:

$$F_i = F_{h_i} + \sum_j F_{p_{ij}};$$

$$F_{P_{ij}} = F_{\mathrm{VanDerWaals_{ij}}} + F_{\mathrm{Born_{ij}}} + F_{\mathrm{volume\_exclusion}} \tag{3}$$

$$M_i = M_{h_i} + a \times \sum_j F_{p_{ij}} \times n_{ij}; \quad n_{ij} = \frac{r_{ij}}{|r_{ij}|} \tag{4}$$

where F_h, M_{hi}, $F_{\mathrm{Van\ Der\ Waals}}$, F_{Born}, $F_{\mathrm{volume\_exclusion}}$, F_p, r_{ij} and n_{ij} are hydrodynamic force, momentum, Van Der Waals attraction, Born repulsion and volume exclusion forces, inter-particle force between two particles, distance vector between two particles and normalized r_{ij}, respectively. The volume exclusion force was calculated according to modified DEM, introduced by Higashitani et al.[11] Van Der Waals attraction and Born repulsion potential can be calculated by using the following equations[14,15]:

$$V_{\mathrm{VanDerWaals}} = -\frac{A}{6}\left(\frac{2a^2}{r^2+4ar} + \frac{2a^2}{(r+2a)^2} + \ln\left(\frac{r^2+4ar}{(r+2a)^2}\right)\right) \tag{5}$$

$$V_{\mathrm{Born}} = 4A\left(\frac{\sigma_c}{a}\right)^6\left(\frac{4!}{10!}\right)\frac{1}{\bar{r}} \times \left[\frac{2(30-\bar{r}^2)}{\bar{r}^7} + \frac{\bar{r}^2+14\bar{r}^2+54}{(\bar{r}+2)^7} + \frac{\bar{r}^2-14\bar{r}^2-54}{(\bar{r}-2)^7}\right] \tag{6}$$

Where A, a, σ_c, r, and $\bar{r}$ are Hamaker constant, particle radius, collision diameter, distance between particle and distance between particles normalized with respect to the particle diameter, respectively. The collision diameter was considered as 0.5 nm.[15] The inter-particle interactions are considered for particles placed within the distance of *4a;* beyond this distance particles have very little influences on each others. The hydrodynamic force and torque applied to particles exposed to the fluid were evaluated by using the following relations:

$$F_{h_i} = \alpha_t 6\pi\mu a(E_i \cdot r_i - V_i) \tag{7}$$

$$M_{h_i} = \alpha_r 8\pi a^3(\omega_0 - \omega_i) \tag{8}$$

where μ is viscosity, E is velocity gradient V_i is the velocity of particle i and ω_0 and ω_i are vorticity vector of flow field at the point where particle i is located and the rotation vector of particle i, respectively. α_t and α_r are correction factors for hydrodynamic force and torque calculated for each particle, respectively. α_t is the ratio of forces acting on the part of the particle surface exposed to the surrounding fluid [see Fig. 1] calculated from $3/2\, a\mu V_R \int_0^{\pi}\int_{\theta_1}^{\theta_2} |\sin\theta| d\theta d\phi$,[16] to the net stocks' force acting on a single particle, $6\pi\mu a V_R$. The torque is assumed to be proportional to the angle of the exposed surface of the particle to the flow and α_r can be given by $|\theta_2 - \theta_1|/2\pi$.[11] In order to avoid burst of calculation, the time step employed was quite small, 10^{-11} to 10^{-12}. The dependence of the calculation time the number of the particles is somehow larger than $N\log N$.

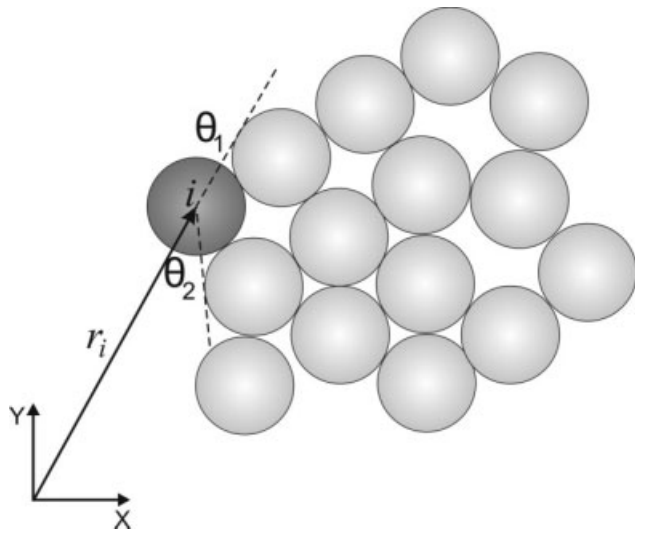

Figure 1 Schematic drawing of particle i whose surface between θ_1 and θ_2 is exposed to the fluid.

Agglomerate structure

Two aggregate structures each composed of 33 particles with structure as shown in Figure 1 were considered. Structure (I) is a fully packed agglomerate with fractal dimension of about 2 [Fig. 2-a]. Structure (II) is constructed using diffusion limited aggregation (DLA) growth mechanism with fractal dimension of 1.66 [Fig. 2-b]. To find stable positions, the aggregates were subjected to the zero flow fields for 10^6 steps. The particle characteristics are given in Table I.

RESULTS AND DISCUSSION

The simulation of aggregate dispersion process was made for three different flow fields namely steady shear flow, elongational flow, and combined shear-elongational flow. In the combined shear and elongational flow the contribution of each flow determined by their second invariants of deformation tensors was considered to be equal. The calculations were preformed for three different stresses, $\tau = \mu\dot{\gamma}$, where $\dot{\gamma}$ represents the second invariant of deformation tensor: 469.575, 939.15, and 1878.3 Pa. The range

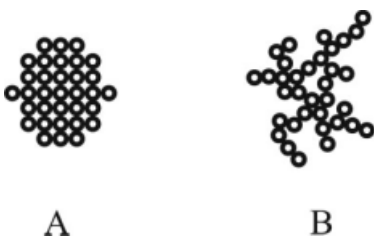

Figure 2 Structures of agglomerate: (A) Structure (I) (B) Structure (II).

TABLE I
The Properties of the Particles

Property	Value	Unit
Density	1.05×10^3	kg m^{-3}
Hamaker constant	1.3×10^{-20}	J
Viscosity of medium	8.4×10^{-4}	Pa S
Radius of particle	100×10^{-9}	m

of stresses considered was high enough to ensure that the flow field is capable of breaking the agglomerate and this range of stress was close to the range used by Higashitani et al.[11] and Fanelli et al.[13,14] As the agglomerate break-up is scaled with strain,[17] to reach the required strain in a reasonable calculation time period, the simulation was performed at high shear rates and low viscosity.

The extent of the aggregate dispersion process was evaluated in terms of weighted average fragment size, $\langle w \rangle$, defined as:

$$\langle w \rangle = \frac{\sum_i i^2 n_i}{\sum_i i n_i} \tag{9}$$

where n_i is the number of aggregate with i particles. For each case $\langle w \rangle$ was plotted against time in order to study the kinetics of dispersion process.

Effect of flow field

Figure 3 compares the snapshots of aggregate dispersion process predicted for shear and elongational flow fields at applied stress $= \mu\dot{\gamma} = 1878.3$ Pa.

As it can clearly be noticed, the dispersion ability of elongational flow field is greater than that of shear flow field such that much smaller fragments can be obtained by elongational flow field.

It can also be observed that in elongational flow field the aggregates are mostly broken down into smaller fragments at the very beginning of the mixing process and no further break down will occur at the later stages of the mixing time. Figure 4 shows the time evolution of the aggregate dispersion

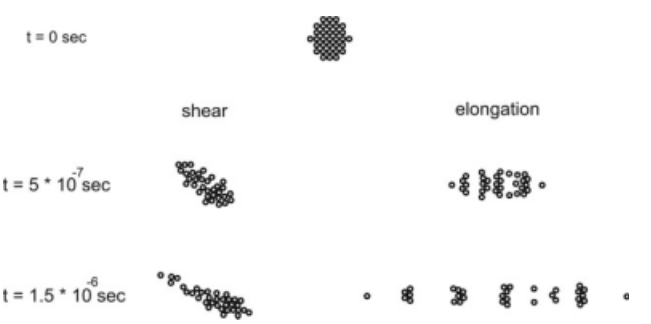

Figure 3 Time evolution of dispersion in shear and elongational flow fields at $\mu\dot{\gamma} = 1878.3$ Pa for structure (I).

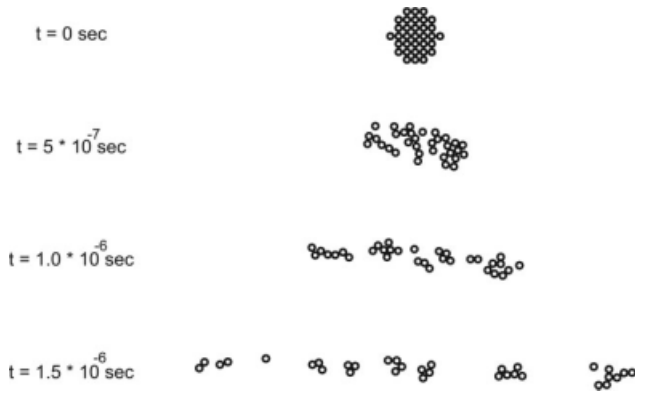

Figure 4 Time evolution of dispersion combined shear-elongational flow fields at $\mu\dot{\gamma} = 1878.3$ Pa for structure (I).

process of structure (I) in the combined shear-elongational flow field. By comparing these results with those shown in Figure 3, one may notice that the aggregate dispersion performance of combined shear-elongational flow fields is greater than shear flow field.

Figure 5 compares the time evolution of the dispersion of the structures (I) and (II) in steady shear flow field with $\mu\dot{\gamma} = 939.15$ Pa. As it is seen, structure (II) is easier to be broken up compared with structure (I) and smaller fragments can be produced with structure (II). This is due to the fact that in this structure more particles are exposed to the flow field

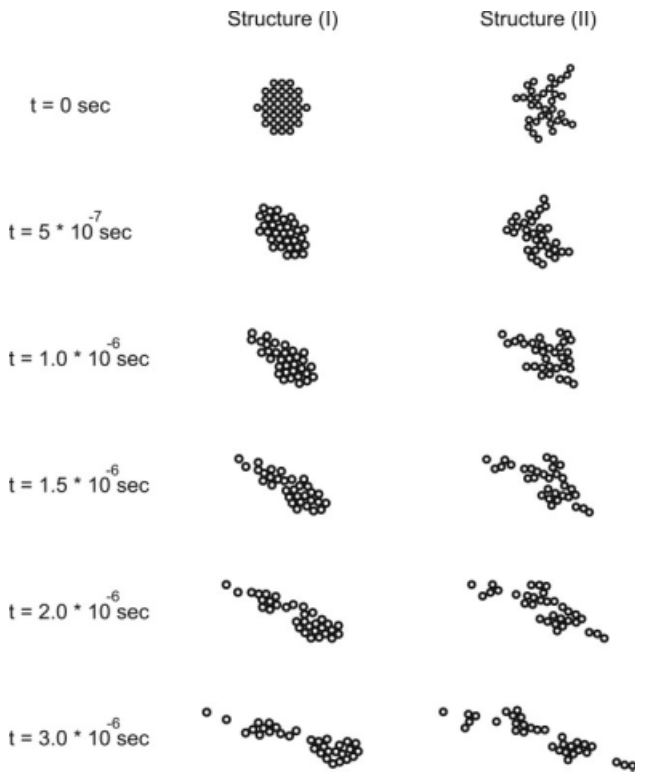

Figure 5 Time evolution of dispersion of structures (I) and (II) in shear flow field with $\mu\dot{\gamma} = 939.15$ Pa.

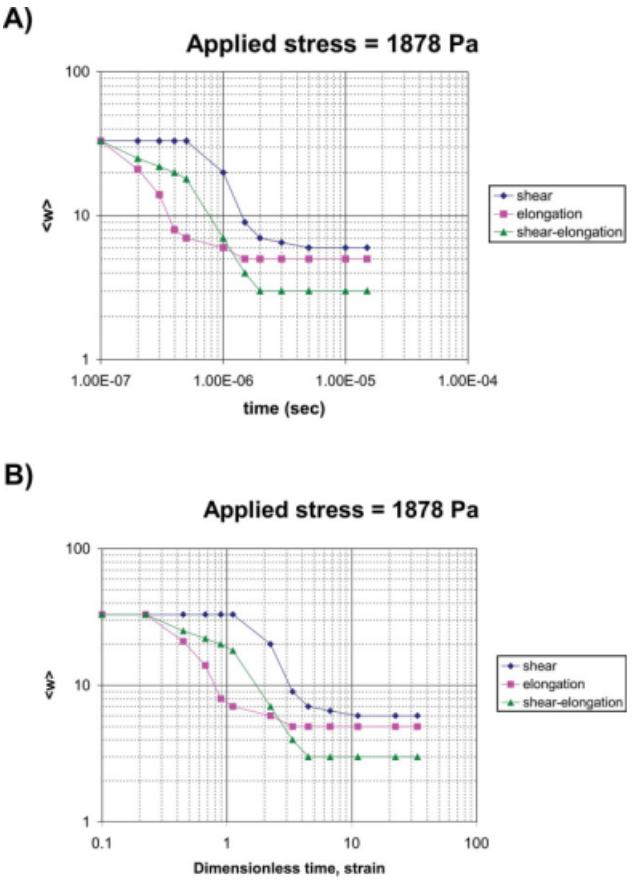

Figure 6 Weighted average fragments size vs. (A) time, (B) dimensionless time, strain, for $\tau = 1878.3$ Pa for agglomerate with structure (I) in different flow fields. [Color figure can be viewed in the online issue, which is available at www.interscience.wiley.com.]

and the contact surface and hence cohesive forces between particles are lower compared with structure (I). More details regarding the effect of aggregate structure on the dispersion process will be discussed in Effect of aggregate structure section.

Figure 6(A) shows the variation of $\langle w \rangle$ as a function of time predicted for three different flow fields for structure (I) in logarithmic scale. These results can provide more insight into understanding the breaking process of agglomerate if they are presented in dimensionless form as shown in Figure 6(B). It can be seen from Figure 6(B) that for the three flow fields the reduction of $\langle w \rangle$ follows a power–law type relation ($\langle w \rangle = k\, t^{-m}$) with time during the period of dispersion process. The corresponding power–law relation values are given in Table II.

It can be noticed that for shear stress $\mu\dot{\gamma} = 1878.3$ Pa, in the elongational flow the aggregate break up process begins quicker and $\langle w \rangle$ reaches to its steady state values at the earlier stage of the mixing time compared with the steady shear flow. The final or steady state fragment size achievable in elongation flow was also found to be smaller than that in shear flow.

TABLE II
The Values of m and $\langle w \rangle_{final}$ predicted for Aggregate with Structures (I) and (II) in Three Different Flow Fields with Various $\mu\dot{\gamma}$

Type of flow		Shear			Elongation			Combined shear-elongation		
Applied stress, $\mu\dot{\gamma}$ (Pa)		1878.3	939.15	469.57	1878.3	939.15	469.57	1878.3	939.15	469.57
Structure-I	$\langle w \rangle_{final}$	6	7	15	5	5	8	3	5	12
	m	0.5656	0.511	0.3465	0.7254	0.6798	0.5696	0.52	0.4784	0.3567
Structure- II	$\langle w \rangle_{final}$	6	7	10	2	3	5	2	5	7
	m	0.5708	0.5221	0.4102	1.166	0.7672	0.6325	0.5233	0.5673	0.6984

The aggregate dispersion process in combined shear-elongational flow field begins as early as elongational flow but proceeds with dispersion rate similar to that of shear flow. These results suggest a greater aggregate dispersing ability for elongational flow field in comparison with shear flow. Moreover, as can clearly be seen in Figure 6, the fragment size predicted in combined shear and elongational flow is much smaller than those predicted for the other two flow fields. This can be explained in term of ability of shear flow field in rotating the aggregate or fragments inappropriate direction to be broken by elongational flow which has a strong ability in breaking the aggregates. In other words, in combined shear-elongational flow field the rate of aggregate dispersion process is controlled by shear flow field as slower breaking process.

Figure 7 shows the simulation results as those shown in Figure 6 for $\mu\dot{\gamma}$ = 939.15 Pa. A similar trend was found for $\mu\dot{\gamma}$ = 939.15 Pa. As it was expected for shear flow field, as the applied stress decreases the rate of aggregate dispersion process decreases and the final fragment size becomes larger. The same trend was observed for combined shear-elongational flow field. However, in contrary to these two flow fields, in elongational flow field, decreasing the applied stress resulted in smaller fragment size. It can be explained by noticing this fact that in lower stresses the dispersion process takes place in lower rates and allows particles or fragments to interact with each other and make the fragments to slightly rotate, rearrange, and align in more appropriate direction for elongational flow where they will be broken up into smaller fragments.

It should be noted that a similar trend as that shown in Figure 7 was found for $\mu\dot{\gamma}$ = 469.575 Pa and is shown in Figure 8.

Effect of aggregate structure

Figure 9 compares the results predicted for aggregate dispersion of structures (I) and (II) at low and high stress levels in shear flow field. The corresponding values of m and $\langle w \rangle$ are given in Table II. As can be noticed, structure (II) shows a similar dispersion behavior as structure (I) at high stress level while they exhibit different behaviors at low stresses.

Moreover, the final weighted average fragment size ($\langle w \rangle_{final}$) predicted for structure (I) at low stress

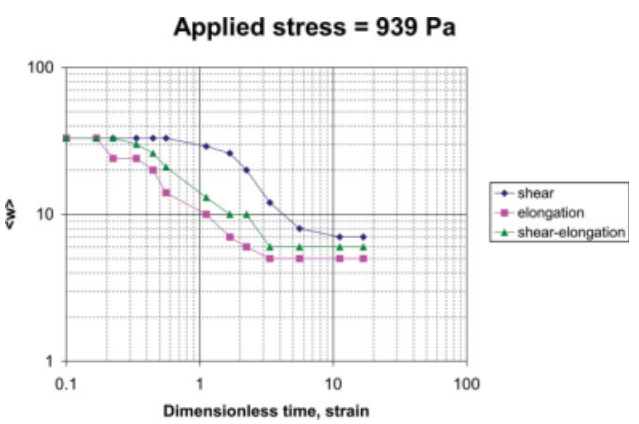

Figure 7 Weighted average fragments size vs. dimensionless time, strain, for τ = 939.15 Pa for agglomerate with structure (I) in different flow fields. [Color figure can be viewed in the online issue, which is available at www.interscience.wiley.com.]

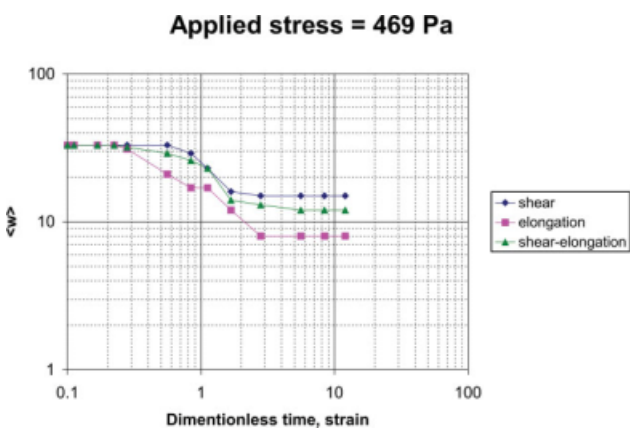

Figure 8 Weighted average fragments size vs. dimensionless time, strain, for τ = 469.575 Pa for agglomerate with structure (I) in different flow fields. [Color figure can be viewed in the online issue, which is available at www.interscience.wiley.com.]

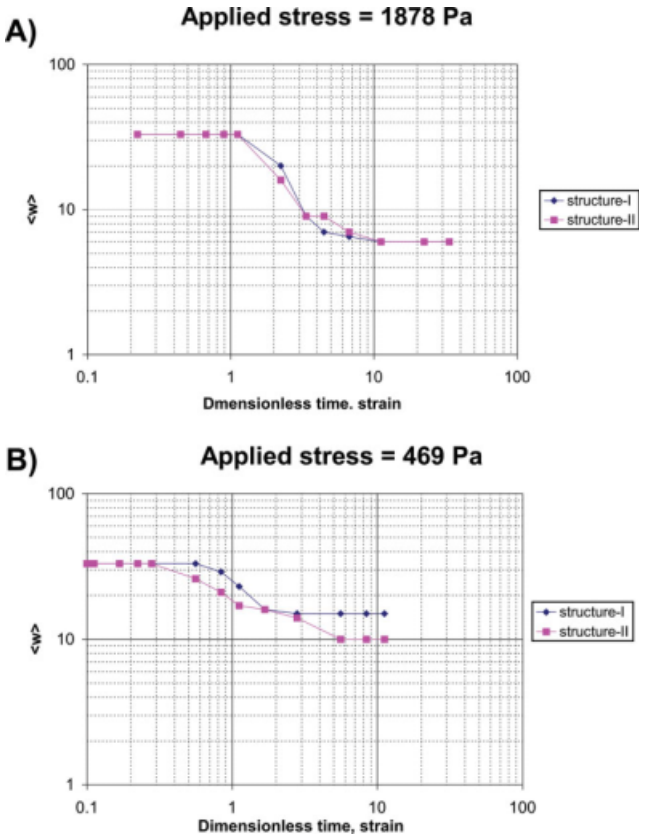

Figure 9 The plot of weighted average fragment size against dimensionless time for Structure (I) (◆) and Structure (II) (■) in different stresses: (A) applied stress τ = 1878.3 Pa (B) applied stress τ = 469.575 Pa. [Color figure can be viewed in the online issue, which is available at www.interscience.wiley.com.]

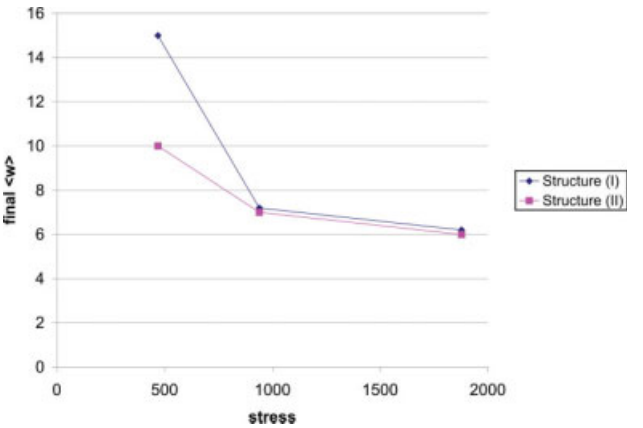

Figure 10 Plot of final weighted average fragment size ($\langle w \rangle_{final}$) vs. applied stress (Pa) for structure (I) (◆) and structure (II) (■). [Color figure can be viewed in the online issue, which is available at www.interscience.wiley.com.]

was higher than that for structure (II), whereas $\langle w \rangle_{final}$ was found to be the same at high applied stresses which is demonstrated in Figure 10. These results can be attributed to the higher contribution of low stresses in dispersion process of structure (II) compared with structure (I) in which high stresses play more significant role in dispersion process. The reason behind this is that the structure (II), in contrary to structure (I), contains domains with lower extent of particle–particle interaction which are easier to be broken at lower stress levels.

Furthermore, from the values of $\langle w \rangle_{final}$ and m given in Table II it was found that, in contrary to shear flow field in which two aggregate structures exhibited similar behavior at high stress level, in elongational flow field the extent of aggregate dispersion was higher for structure (II) in whole stress ranges.

The dispersion of aggregates with structures (I) and (II) at different applied stresses in combined shear-elongational flow field as a function of time are shown in Figure 11(A,B), respectively. These results reveal that for structure (II) the rate of aggregate dispersion is higher and the final fragment size is lower in comparison with structure (I). It is interesting to note that in structure (II), in contrary to structure (I), the rate of aggregate dispersion increases with decreasing the total applied stress in this particular flow field. This is because in structure (II) at high stresses, there are weak segments which

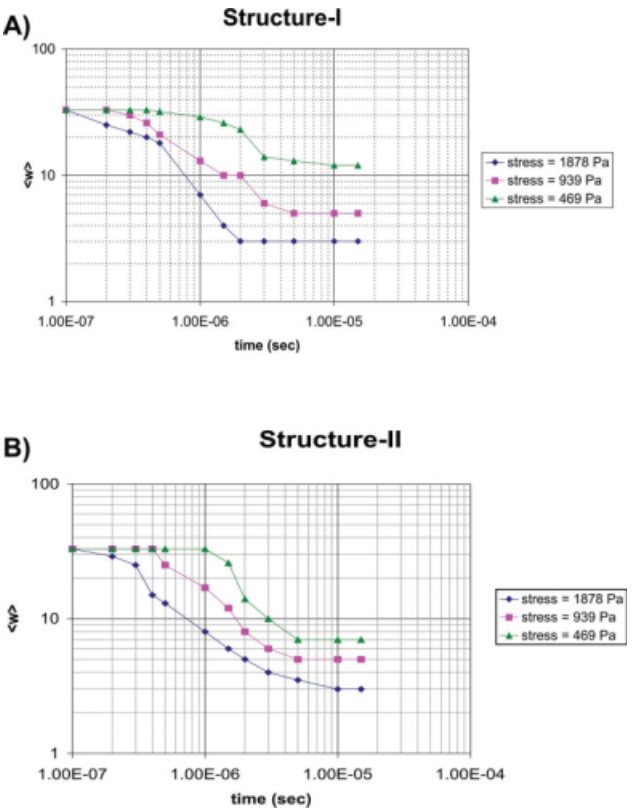

Figure 11 Plot of weighted average fragment size ($\langle w \rangle$) against time for combined shearelongational flow field: (A) structure (I) (B) structure (II). [Color figure can be viewed in the online issue, which is available at www.interscience.wiley.com.]

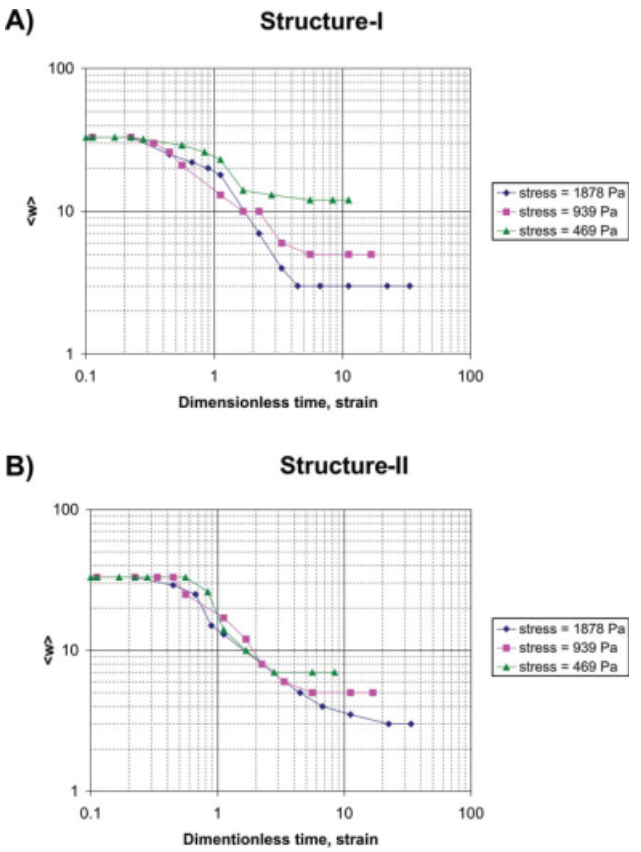

Figure 12 Plot of weighted average fragment size ($\langle w \rangle$) against dimensionless time, strain, for combined shear-elongational flow field: (A) structure (I) (B) structure (II). [Color figure can be viewed in the online issue, which is available at www.interscience.wiley.com.]

can easily be broken and separated from the parent aggregate at the early stages of the dispersion process, while at low stresses the aggregate is first rearranged into a new structure in which most of its segments have close break-up strength. Plots of $\langle w \rangle$ as a function of dimensionless time, strain, in Figure 12 shows that structure (II) breaks at higher strains compared with structure (I). It can be attributed to the loose structure of structure (II) which causes agglomerate to deform to greater extents and breaks up at higher strains, whereas structure (I), because of its dense and packed structure, cannot deform as high as structure (II) and breaks up at lower strains than that for structure (II). Results shown in Figure 12(B) also show that at high stresses, structure (II) breaks at lower strains than that for low stresses. This is because at high stresses or high deformation rates, the agglomerate does not have enough time to be deformed and therefore breaks at lower strains.

From the results discussed earlier, it was found that there is a time period prior to aggregate break-up process whose extent was found to be depended on aggregate structure, type of flow field, and level of applied stresses. This time period was found to be decreased with decreasing fractal dimension and increasing applied stress. This is the issue of our present study and will be explained in our future works.

CONCLUSION

It was demonstrated that the extent as well as the rate of the aggregate dispersion (or break-up) process in three different flow fields namely steady shear, elongation flow, and combined shear and elongational flow fields, can be predicted by utilizing the DEM. Results of the simulation showed that the aggregate dispersion process, evaluated in terms of weighted average fragment size $\langle w \rangle$, follows a similar power law relation with time as $\langle w \rangle = k\ t^{-m}$ in the period of dispersion for all three flow fields considered. In the range of stresses considered (469–1878 Pa), the dispersion of aggregates exposed to the elongational flow was found to begin quicker and reach to its steady state values at the earlier stage of the mixing time compared with shear and combined shear and elongational flow fields. The dispersion performance of different flow fields determined in terms of dispersing rate and a final steady state fragment size was found to be dependent upon the extent of applied stress and flow fields such that, at low applied stress levels, much smaller steady state values of $\langle w \rangle$ could be obtained for the elongational flow. Finally, the aggregate structure characterized by their fractal dimension was found to have different effects on the aggregate dispersion process depending on the flow field and applied stress level. The results predicted from this simulation could be explained in terms of the ability of flow fields in rotating the aggregates and fragments in appropriate position to be broken up and the fractal dimensions of aggregates. It was also shown that the agglomerate with lower fractal dimensions deforms to greater extent before breaking up compare with those with higher fractal dimension due to their loose structure.

References

1. Powell, R. L.; Mason, S. G. AIChE J 1982, 28, 286.
2. Shiga, S.; Furuta, M. Rubber Chem Tech 1984, 58, 1.
3. Feke, D. L.; Manas-Zloczower, I. Chem Eng Sci 1991, 46, 2153.
4. Hansen, S.; Khakhar, D. V.; Ottino, J. M. Chem Eng Sci 1998, 53, 1803.
5. Horwatt, S. W.; Manas-Zloczower, I.; Feke, D. L. Chem Eng Sci 1992, 47, 1849.
6. Rwei, S. P.; Manas-Zloczower, I.; Feke, D. L. Polym Eng Sci 1990, 30, 701.
7. Rwei, S. P.; Manas-Zloczower, I.; Feke, D. L. Polym Eng Sci 1991, 31, 558.
8. Boisses, G.; Brady, J. F. J Fluid Mech 1985, 155, 105.

9. Cunsall, P. A.; Strack, O. D. L. Geotechnique 1979, 29, 47.
10. Cundall, P. A. U.S. Army Corps of Engineering (Missouri River Division), Tech. Rep. MRD-2074, 1974.
11. Higashitani, K.; Iimura, K. J Colloid Interface Sci 1998, 204, 320.
12. Higashitani, K.; Iimura, K.; Sanda, H. Chem Eng Sci 2001, 56, 2927.
13. Fanelli, M.; Manas-Zloczower, I.; Feke, D. L. Polymer Processing Society Annual Meeting (PPS-20).
14. Fanelli, M.; Manas-Zloczower, I.; Feke, D. L. Chem Eng Sci 2006, 61, 473.
15. Elimelech, M.; Gregory, J.; Jia, X.; Williams, R. A. Particle Deposition and Aggregation: Measurement, Modeling, Simulation, Butterworth-Heinemann: Oxford, 1995.
16. Bird, R. B.; Stewart, W. E.; Lightfoot, E. N. Transport Phenomena; Wiley: New York, 1960; p 56.
17. Scurati, A.; Manas-Zloczower, I.; Feke, D. L. Chem Eng Sci 2005, 60, 6564.